

Design and laboratory testing of a MEMS accelerometer array for subsidence monitoring

Chunying Xu, Jiawang Chen, Huangchao Zhu, Peihao Zhang, Ziqiang Ren, Hai Zhu, and Yuan Lin

Citation: *Review of Scientific Instruments* **89**, 085103 (2018); doi: 10.1063/1.5036666

View online: <https://doi.org/10.1063/1.5036666>

View Table of Contents: <http://aip.scitation.org/toc/rsi/89/8>

Published by the American Institute of Physics

Articles you may be interested in

New design techniques of resistive bolometer system for analysis of total radiated power

Review of Scientific Instruments **89**, 083501 (2018); 10.1063/1.5026927

Apparatus and method for the growth of epitaxial complex oxides on native amorphous SiO₂ surface of (001) oriented single crystal silicon

Review of Scientific Instruments **89**, 085102 (2018); 10.1063/1.5040390

Multispectral medical image fusion scheme based on hybrid contourlet and shearlet transform domains

Review of Scientific Instruments **89**, 084301 (2018); 10.1063/1.5016947

Note: Lever-type bidirectional stick-slip piezoelectric actuator with flexible hinge

Review of Scientific Instruments **89**, 086101 (2018); 10.1063/1.5038640

A comparison based digital waveform generator for high resolution duty cycle

Review of Scientific Instruments **89**, 084101 (2018); 10.1063/1.5004798

A practical wide-field Raman imaging method with high spectral and spatial resolution

Review of Scientific Instruments **89**, 083103 (2018); 10.1063/1.5041529



Design and laboratory testing of a MEMS accelerometer array for subsidence monitoring

Chunying Xu, Jiawang Chen,^{a)} Huangchao Zhu, Peihao Zhang, Ziqiang Ren, Hai Zhu, and Yuan Lin

Ocean Collage, Zhejiang University, Zhoushan 316021, China

(Received 17 April 2018; accepted 9 July 2018; published online 3 August 2018)

The *in situ* monitoring of displacement variation is important for studying the seabed subsidence mechanism. To meet the multi-point measurement requirements for vertical displacement in subsidence monitoring of the seabed surface, a Micro-Electro-Mechanical Systems accelerometer array was designed. By sensing the tilt angles, displacements on the array can be calculated. The subsidence is calculated as the difference in the displacements from the initial values. To improve the accuracy of the displacement calculation, a calibration model of the tilt angle was presented. The model parameters are computed through a least squares estimation method, which is solved by the Levenberg-Marquardt algorithm. Experimental results show that the calibration model performs excellently with the maximum error of tilt angle being less than 1° in the measurement range (-90°, 90°). The displacement measurement accuracy of the array (2.1 m long) is almost less than 1 cm. Thus, the results show a strong agreement between the detected data and actual deformation in the test. Published by AIP Publishing. <https://doi.org/10.1063/1.5036666>

I. INTRODUCTION

Seabed subsidence is an environmental geology phenomenon, which can cause various disasters, such as destruction of ocean platforms, destruction of oil wells, or even gas blowouts.^{10,13,24,28} Researchers have conducted considerable simulation studies on seabed deformation subsidence.^{8,26,27,30} For example, the range of subsidence would be from 10 cm to 30 cm around the gas hydrate production well according to a simulation from the Japan OYO Corporation. The estimated subsidence around the well would be approximately 10 cm for a 10-day production.^{26,27} Therefore, it is of great value to conduct research on and develop an *in situ* system for seabed subsidence monitoring.

In terms of seabed deformation, *in situ* monitoring methods remain sparse.²³ A servo-accelerometer is used to monitor seabed stability during methane hydrate production, where seabed deformation was calculated using the double-integral method.¹⁹ However, the integral method requires the initial conditions of the displacement to be determined, which are generally unavailable.¹⁴ This method was not applied during the production test of methane hydrate in 2012. Pressure sensors are often applied to measure seabed subsidence or uplift during methane hydrate production. The pressure sensor is based on quartz strain gauge technology, which can detect the pressure shift associated with the subsidence or uplift of the seabed with an accuracy of 10 mm.^{12,21} The pressure gauges deployed on the seabed can continuously monitor changes in overlying water pressure, with seabed subsidence recorded as a pressure increase and seabed uplift recorded as a pressure decrease. However, this method is not appropriate in shallow seas because pressure records are too noisy for reliable analysis, owing to near-coastal oceanographic signals.²³ However,

most quartz pressure gauges undergo a drift at unpredictable rates that is typically equivalent to 20 cm per year.¹⁷ Moreover, all of these are spatially restricted because they adopt single-point sensors.²³

On the other hand, the stratigraphic horizontal displacement is an important monitoring parameter for landslides. In a landslide monitoring system, a sensor array is mounted vertically into the boreholes, measuring the horizontal displacement. While the monitoring of subsidence is to measure the vertical displacement, a sensor array is required to be deployed horizontally. So, *in situ* displacement measuring instruments for landslides in the field can be used as important references, for example, fibre Bragg grating (FBG) inclinometers and Micro-Electro-Mechanical Systems (MEMS) inclinometers or accelerometers.²⁹ FBG is a new method for measuring landslide displacement in which the instrument is buried in the landslide for mapping the deformation information through the modulation and analysis of optical signal transmission changes in the FBG circuits.^{2,15,16,29} However, the measurement results are greatly influenced by the embedding process. Furthermore, it is difficult to form a standard quantitative measurement based on the strain of a reference plate, a column, a pipe, and even the line to measure the conversion amount, and the conversion from strain to displacement is not determined. In principle, the cable or FBG must be tight when buried and is thus in danger of snapping during deformation, especially when the soil is soft.²⁹ With the development of the MEMS technology, MEMS inclinometers and accelerometers have been used in landslide detection for measuring horizontal displacement^{20,22,29} with the characteristics of small size, low power consumption, and high reliability.¹⁸ MEMS accelerometers are used to monitor ground subsidence caused by underground excavation in the construction of tunnels. The system considered the change in tilt angles at the survey points rather than the subsidence displacements.⁹ A shape accel array (SAA)

^{a)}Author to whom correspondence should be addressed: arwang@zju.edu.cn

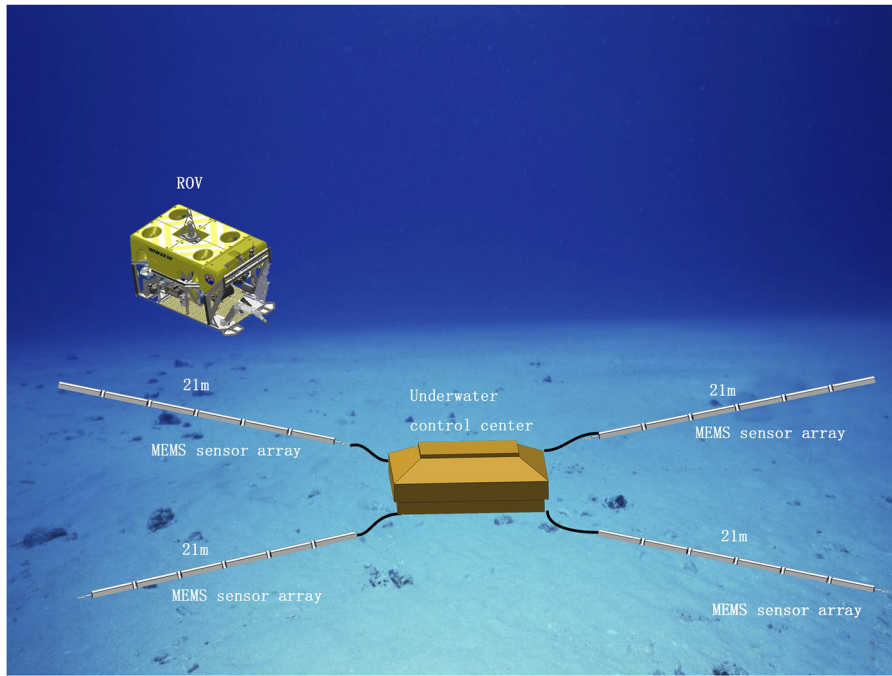


FIG. 1. Schematic diagram of the sensor arrays for seabed subsidence monitoring.

which was manufactured by Measurand, Inc. (Canada) consists of a rope-like array of triaxial MEMS-chip accelerometers used to measure deformation or vibration. The SAA measures the shape of a path in boreholes and structures and monitors deformation of land-based structures and slopes.^{1,3,4} Based on the principle of the inclinometers used for horizontal displacement monitoring, in this paper, we developed a MEMS accelerometer array for subsidence measurement. Compared to the pressure sensors, the array has the following features: it is convenient for multi-point deployment with the small size and low power consumption and has high anti-interference capability of noise even in shallow seas with high reliability, overcoming the disadvantages of pressure gauges.

As shown in Fig. 1, the system will be applied to monitor the subsidence in a production test zone of gas hydrate in the South China Sea. Four sensor arrays will be deployed in the shape of “x.” The monitoring range is $30\text{ m} \times 30\text{ m}$. Each array is 21 m. The system will be deployed and recovered by a Remote Operated Vehicle (ROV).

The main contents of this paper include the basic measuring principle for the subsidence (vertical displacement), the composition of the monitoring system, the auto-calibration of the sensor by parameter estimation, and the measurement accuracy of the MEMS array in a laboratory test.

II. MEASURING PRINCIPLE

A. Calculation of tilt angles

As shown in Fig. 2, the sensor local reference system is $[O, X_{MEMS}, Y_{MEMS}, Z_{MEMS}]$, the axes X_{MEMS} and Y_{MEMS} are lying on the sensor surface, and the Z_{MEMS} -axis is orthogonal to the surface. The tilt angle is the angle between the X_{MEMS} -axis and the horizontal plane and is 0° when the Z_{MEMS} -axis is straight up and 90° when the Z_{MEMS} -axis is horizontal.

The calculation of the tilt angle in this paper is based on the assumption that the sensor, in a static condition, is subjected only to the gravity force. That is to say, the module of the acceleration vector $A^T = [a_x, a_y, a_z]$ measured by the sensor has to be equal to the gravitational acceleration g , independent of the sensor orientation,^{5,18} which can be expressed as

$$g = \sqrt{a_x^2 + a_y^2 + a_z^2}, \quad (1)$$

where a_x , a_y , and a_z are the three components of acceleration. The tilt angle α is obtained as⁷

$$\begin{aligned} \alpha &= \sin^{-1}(-a_x/g) \\ &= \sin^{-1}(-a_x/\sqrt{a_x^2 + a_y^2 + a_z^2}). \end{aligned} \quad (2)$$

B. Measurement of the multi-point subsidence by the accelerometer array

The accelerometer cannot obtain the displacement of the subsidence directly; rather, it measures the tilt angles and tendency of the carrier and obtains the displacement by assuming that the deflection angle of the carrier within a finite length l can be approximated to the same value. So, the first step in this calculation was to confirm the status of sensors (i.e.,

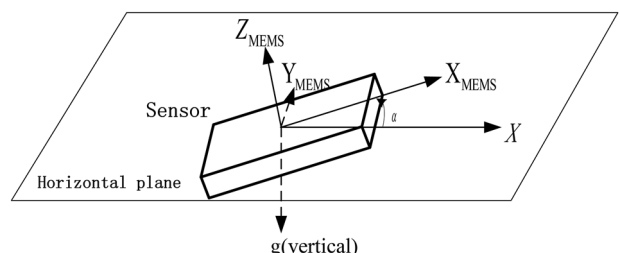


FIG. 2. The tilt measurement from the accelerometer.

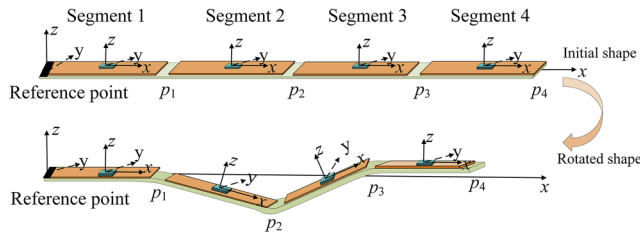


FIG. 3. The principle of the subsidence calculation and calculation of displacement through the tilt angles.

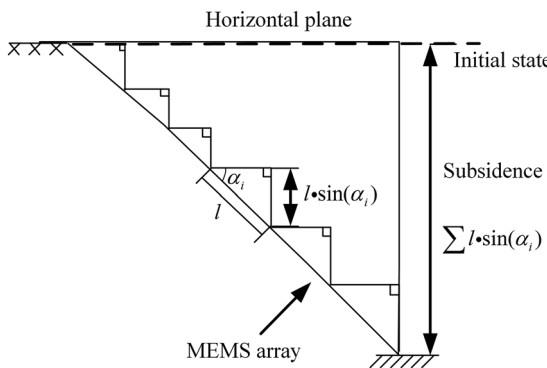


FIG. 4. Schematic diagram of the cumulative displacement curve.

tilt angles) in a stationary state by analyzing how the triaxial acceleration distributes in the gravity field. Therefore, the vertical displacement in length l can be determined,

$$\begin{cases} p_x = l \cos(\alpha) \\ p_y = 0 \\ p_z = l \sin(\alpha) \end{cases}, \quad (3)$$

where α is the tilt angle of a segment.

As shown in Fig. 3, the subsidence body is divided into n segments along the horizontal direction according to the interval l , and the sensor array consists of n units in series connection (the structure of the array is introduced in Sec. III). The length of each segment l is known, 30 cm in the study. For the entire multi-segment MEMS accelerometer array, the coordinate values of each segment were calculated by accumulating the former segments' coordinate values one by one (Fig. 4). To ensure precise measurements, the first segment (i.e., the reference point) must be motionless, and the coordinate values of the reference point are $P_1 = [p_{1.x}, p_{1.y}, p_{1.z}]^T = [0, 0, 0]^T$. So, the tail end of the i th segment, $P_i = [p_{i.x}, p_{i.y}, p_{i.z}]$, can

be obtained by iterative calculation of Eq. (3), which can be expressed as follows:

$$\begin{cases} p_{i.x} = \sum_{j=1}^i l \cos(\alpha_j) \\ p_{i.y} = 0, \quad j = 1, \dots, i; i = 1, \dots, n, \\ p_{i.z} = \sum_{j=1}^i l \sin(\alpha_j) \end{cases} \quad (4)$$

where j is the number of each unit under unit i ; the number of units at the left is 1 and increases by one along the axis; and the right unit displacement is the vertical displacement when $i = n$.

The subsidence is calculated as the difference in coordinate values from the initial values. In this study, the array of the initial state is in the horizontal plane and the initial values are zero, so the coordinate values P_i are the amount of subsidence.

III. COMPOSITION OF THE MONITORING INSTRUMENT

The whole measurement device includes a sensor array, a controller, and a PC (personal computer) code. The sensor array consists of multi-rigid segments (Fig. 5). Each segment hosts a triaxial MEMS accelerometer and is arranged on an elastic steel tape, being fixed to adjoining segments. The width of the tape is 2 cm and the thickness is 1 mm, which allows bends (the bend angle is $[-90^\circ, 90^\circ]$) but resists twisting motions. The length of the array and the length of the segment can be customized depending on the specific application conditions. Generally, the shorter the length of the segment is, the closer it will be to the real situation (the monitoring error is smaller). However, increasing the number of sensors would cause a much more complex acquisition system and cost. In application, both the accuracy and the economical efficiency need to be considered.

The controller is a microcontroller unit (MCU) which is STM32 in the study. Data are acquired from the sensor array by Inter-Integrated Circuit (IIC) bus protocol (at 400 kHz) and sent to the MCU. Then the MCU communicates with the PC software via a RS-232C serial interface at a speed of 115 200 baud. The function of the PC code is to calculate and draw the shape curves of the array, showing directly the amount of vertical deformation and the orientation (subsidence or uplift), giving a visual feedback.

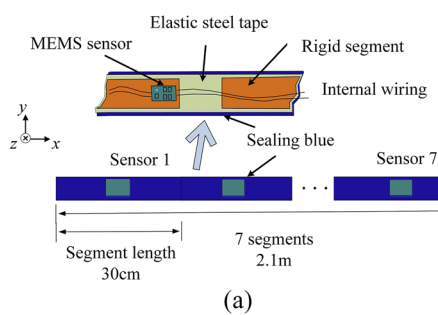


FIG. 5. (a) The structural diagram of the MEMS sensor array; (b) the photo of the sensor array and the MicroController Unit (MCU).

IV. CALIBRATION OF THE MEMS ACCELEROMETER

The measurement results of tilt angles determine the calculation accuracy of the subsidence. But MEMS accelerometers are only approximately calibrated by manufacturers, and on-the-field calibration is necessary to obtain a satisfying accuracy.^{5,6,18} Calibration is aimed at estimating the parameters of a mathematical model, which relates the acceleration sensed by the MEMS accelerometer to the voltage output. It is also based on the assumption that the accelerometer, in the static condition, is subjected only to the gravity force. The accelerometer raw measurements are denoted as $\mathbf{A}' = [a'_x, a'_y, a'_z]^T$. The relationship between the ideal acceleration vector $\mathbf{A} = [a_x, a_y, a_z]^T$ and the accelerometer raw measurements $\mathbf{A}' = [a'_x, a'_y, a'_z]^T$ can be expressed as

$$\mathbf{A} = \mathbf{S}(\mathbf{A}' - \mathbf{O}), \quad (5)$$

where \mathbf{S} is the 3×3 sensitivity matrix and $\mathbf{O} = [o_x o_y o_z]^T$ is the offset vector. The diagonal elements of \mathbf{S} represent the scale factors along the three axes. The other elements of \mathbf{S} are called cross-axis factors. These terms allow describing the axis misalignment, the cross-axis sensitivity, and the mechanical imperfection effect between different channels caused by the sensor electronics. For an ideal accelerometer, the cross-axis factors should all be equal to zero, but for a real one, they can be as large as 2% of the sensor sensitivity.⁵ Imposing the symmetry constraint on the sensitivity matrix \mathbf{S} (that is, $\mathbf{S} = \mathbf{S}^T$), then Eq. (5) can be expressed as

$$\begin{bmatrix} a_x \\ a_y \\ a_z \end{bmatrix} = \begin{bmatrix} s_{xx} & s_{xy} & s_{xz} \\ s_{xy} & s_{yy} & s_{yz} \\ s_{xz} & s_{yz} & s_{zz} \end{bmatrix} \begin{bmatrix} a'_x - o_x \\ a'_y - o_y \\ a'_z - o_z \end{bmatrix}. \quad (6)$$

The model has nine independent parameters: $\{s_{xx}, s_{xy}, s_{xz}, s_{yy}, s_{yz}, s_{zz}, o_x, o_y, o_z\}$.

As mentioned earlier, the tilt angle is the important parameter to calculate the subsidence of the array. The error of the tilt angles e_α can be defined as

$$e_\alpha = |\alpha - \alpha_0|, \quad (7)$$

where α is calculated by Eq. (2) and α_0 is the actual tilt angle. The sensor is placed in N random positions in the range of tilt (-90° , 90°), and record the sensor output $\mathbf{A}' = [a'_x, a'_y, a'_z]^T$ and α_0 , while the sensor is kept in a static condition. A typical method to solve this optimization problem is to minimize the error in a least squares method,

$$\begin{aligned} P(s_{xx}, s_{xy}, s_{xz}, s_{yy}, s_{yz}, s_{zz}, o_x, o_y, o_z) \\ &= \arg \min \sum_{i=1}^N e_{\alpha,i}^2 \\ &= \arg \min \sum_{i=1}^N |\alpha_i - \alpha_{0,i}|^2 \\ &= \arg \min \sum_{i=1}^N (\alpha_i - \alpha_{0,i})^2, \end{aligned} \quad (8)$$

where α_i and $\alpha_{0,i}$ are the calculated and real tilt angles in the i th measurement, respectively.

Here we adopt the Levenberg-Marquardt method, an iterative first-order algorithm that guarantees almost quadratic convergence.¹¹ Starting from an initial guess of the sensor parameters (the nominal values provided by the manufacturer are generally a good choice), the parameters are updated at each iteration as

$$\mathbf{X}^{t+1} = \mathbf{X}^t - [\mathbf{J}(\mathbf{X}^t)^T \mathbf{J}(\mathbf{X}^t) + \lambda D(\mathbf{X}^t)]^{-1} \cdot \mathbf{J}(\mathbf{X}^t)^T \mathbf{r}(\mathbf{X}^t), \quad (9)$$

where \mathbf{X}^t is an unknown vector at the t th iteration, containing the bias vector and the six independent elements of the scale factor matrix: $\mathbf{X}^t = [x_1, \dots, x_9] = [s_{xx}, s_{xy}, s_{xz}, s_{yy}, s_{yz}, s_{zz}, o_x, o_y, o_z]^T$. Let us define the error function $E = \sum_{i=1}^N (\alpha_i - \alpha_{0,i})^2 \cdot r(\mathbf{X}^t)$ and $\mathbf{J}(\mathbf{X}^t)$ are, respectively, the vector of the residuals of $e_{\alpha,i}$ and the Jacobin matrix of the error E , defined as

$$\mathbf{r}(\mathbf{X}^t) = [e_{\alpha,1}, \dots, e_{\alpha,N}]^T, \quad (10)$$

$$\mathbf{J}(\mathbf{X}^t) = \left[\frac{\partial E}{\partial x_1}, \dots, \frac{\partial E}{\partial x_9} \right]. \quad (11)$$

$D(\mathbf{X}^t)$ is a diagonal matrix, whose diagonal coincides with the diagonal of $\mathbf{J}(\mathbf{X}^t)^T \mathbf{J}(\mathbf{X}^t)$; the scalar factor λ in Eq. (9) is a damping factor that avoids singularities in the inversion of $\mathbf{J}(\mathbf{X}^t)^T \mathbf{J}(\mathbf{X}^t)$: it does not affect the final solution, but it does influence the convergence speed.¹⁸ Here it has been set experimentally to $\lambda = 10^{-6}$.¹¹ The iterative procedure is repeated until convergence, which is reached here when the largest parameter change between \mathbf{X}^{t+1} and \mathbf{X}^t is smaller than 10^{-6} .

Once the parameter estimation procedure has been completed, the tilt angles after calibration can be calculated according to Eq. (2). In short, the calibration procedure could be concluded in three steps: (1) collecting samples of tilt angles, (2) computing the model parameters by the least squares estimation method; and (3) using the estimated parameters to compute tilt angles.

V. EXPERIMENTAL TEST AND RESULTS

A. Calibration results

To evaluate the performance of the calibration model, real tilt angles are needed for calculating the model parameters and evaluating the accuracy. In our experimental setting, we collect sample tilt angles using a digital protractor shown in Fig. 6.

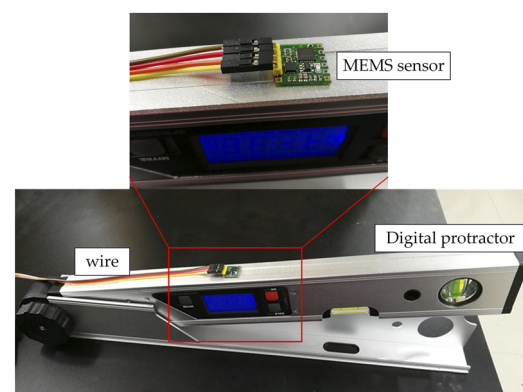


FIG. 6. The protractor for measuring the tilt angles of the MEMS sensor.

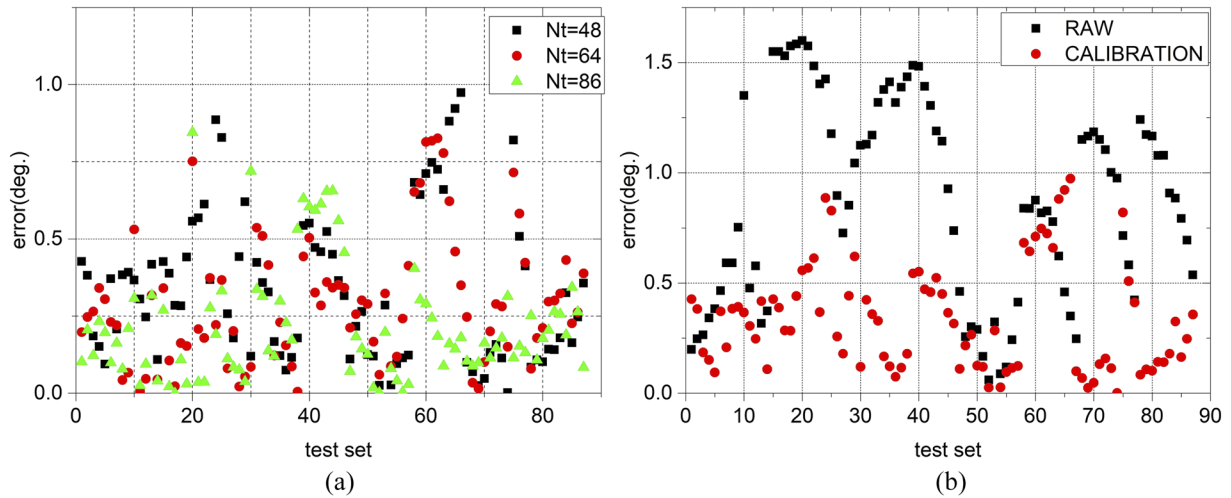


FIG. 7. Errors of our model with different sized samples ($^{\circ}$). The size of the test set for tilt is 87. (a) Errors of tilt angles with 48, 64, 86 samples by the calibration method. (b) Errors of the tilt angles with calibration and without calibration (RAW).

The protractor can provide the indication of the tilt angles with an accuracy of 0.1° .

We collect groups of the tilt angles and outputs of the MEMS accelerometer $\{\alpha_0, \alpha'_x, \alpha'_y, \alpha'_z\}$ to test the performance of our model. The measurement range of our tilt sensing is $(-90^{\circ}, 90^{\circ})$. In order to exclude observational errors, average data in 8 samples at a position are used. According to Ref. 25, a training set of 48 samples is feasible. In this study, different sizes of training sets (N : the size of training set, $N = \{48, 64, 86\}$) are applied to obtain the model parameters and verify the error of tilt angles defined in Eq. (7) on another test set (the size is 87). The results are illustrated in Fig. 7. We can see that the errors of tilt angles are reduced to less than 1° . From Fig. 7(a), it can be concluded that without demanding too high accuracy, 48 samples could be feasible. For higher accuracy, the 86 samples could be applied. Fig. 7(b) shows the errors of the tilt angles by RAW (without calibration) and calibration methods. The size of the training set is

86. The error of tilt angles can be reduced effectively after calibration.

B. Accuracy of the subsidence measurement

In the test, seven MEMS accelerometers (7 segments) are used to reconstruct shapes of the array. The sensor array is deployed on the floor. Black bricks in Fig. 8 are used to generate the shapes of the array. End points of seven segments are selected for tested points. The reference point selected is the first point of the first segment. To validate the monitoring accuracy, the Hexagon WLS400M white light scanner system is applied, which includes high-resolution digital cameras, LED-based illumination, carbon fibre structure, and rapid data-acquisition and processing. The accuracy of the WLS400M system is 0.03 mm. The process is as follows: The Hexagon WLS400M system projects a random pattern on the array and triggers a simultaneous capture of the area of interest by its cameras. The images are correlated using proprietary algorithms to create a three-dimensional point cloud representation of the array. The outputs of the WLS400M system represent the actual displacements of the test points. At the same time, the MEMS accelerometer measures the static acceleration, and then the data are collected by the MCU, sent to the PC, and are transferred to tilt angles. Then the shapes of the array are

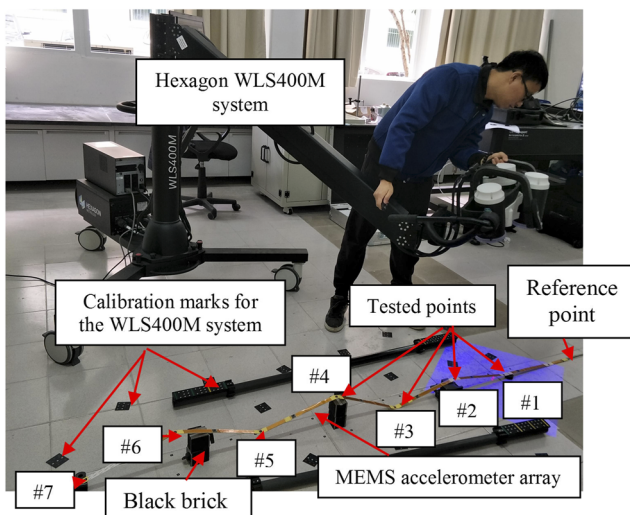


FIG. 8. The MEMS accelerometer array and the Hexagon WLS400M system.

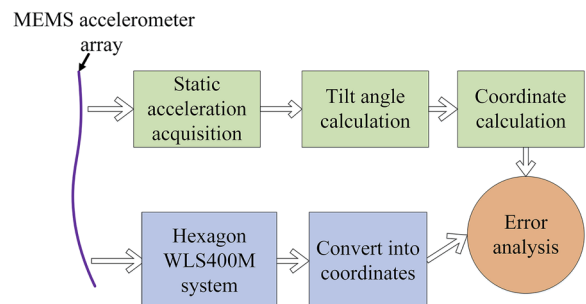
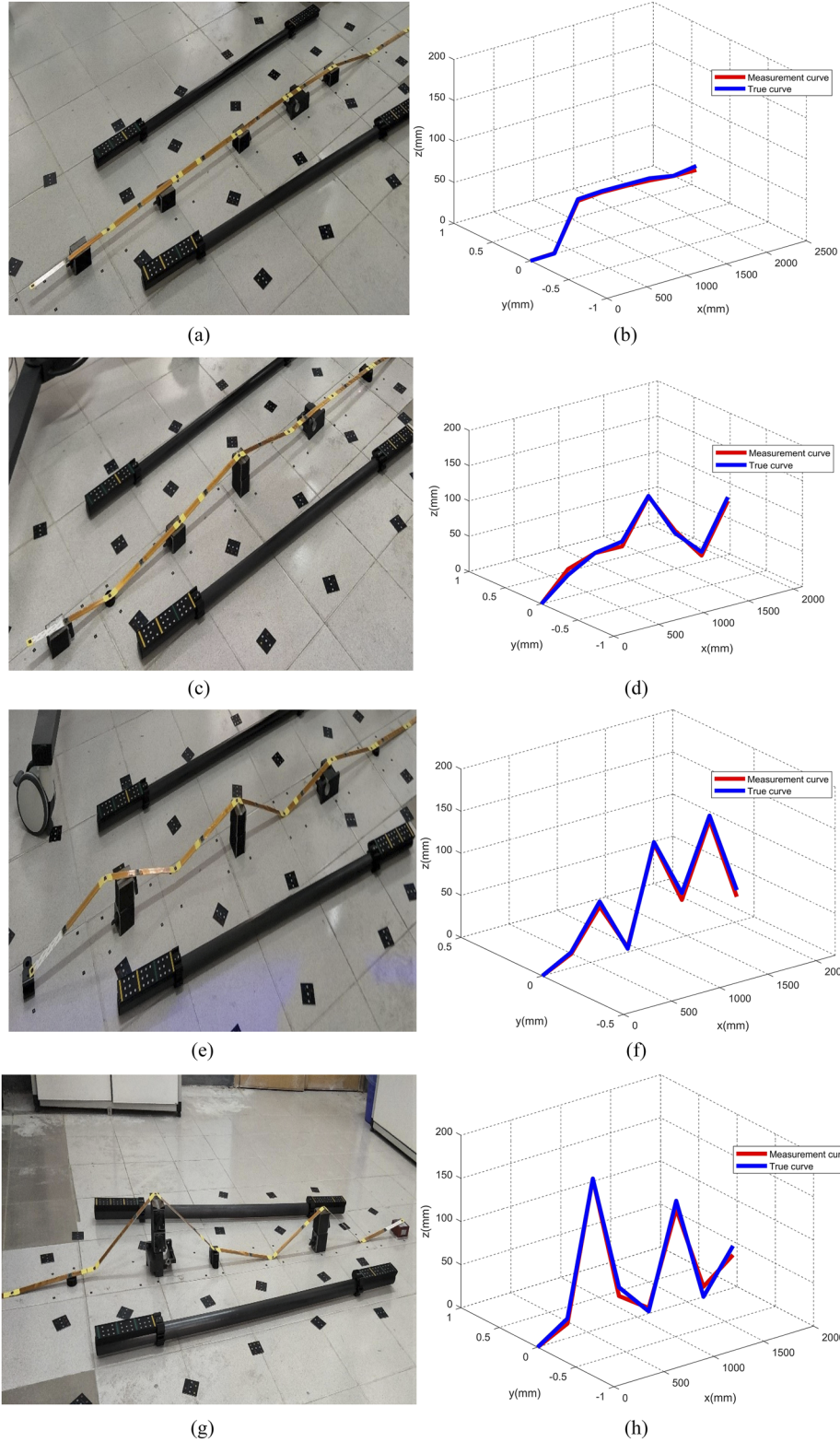


FIG. 9. Error analysis principle for shape reconstruction of the MEMS accelerometer array.

obtained according to the relationship of the tilt angles and coordinates mentioned earlier [Eqs. (2) and (4)]. The reference point and tested points are the same for the system developed and the Hexagon WLS400M. Then the reconstruction error can be obtained by estimating the displacement difference between the two methods. Error analysis principle for shape reconstruction of the MEMS accelerometer array is shown in Fig. 9.



As mentioned earlier, the initial values of the array are zero, the displacements measured directly represented the amount of vertical deformation. We test four different states which are shown in Figs. 10(a), 10(c), 10(e), and 10(g). The respective measurement curves (calculated by the data from the sensors) and the true curves (measured by the Hexagon WLS400M system) are shown in Figs. 10(b), 10(d), 10(f), and 10(h). The mean absolute error (MAE), root-mean-square

FIG. 10. Four shapes for analyzing the construction effect: (a), (c), (e), and (g) are the photos of shapes 1-3; (b), (d), (f), and (h) are the curves obtained from the two methods. Red lines are the measurement curves from the MEMS accelerometers, and blue lines are the true curves obtained from the Hexagon WLS400M system.

TABLE I. The measurement error.

	Mean absolute error (mm)	Root mean square error (mm)	Maximum absolute error (mm)	Maximum deformation (mm)	Minimum deformation (mm)	Maximum tilt angle (deg)	Minimum tilt angle (deg)
Shape1	1.59	2.35	5.04	61.99	0.53	11.15	-0.10
Shape2	3.78	4.82	8.25	113.13	6.01	-12.9	1.15
Shape3	4.16	5.17	8.55	133.91	17.48	-23	3.25
Shape4	6.43	8.31	11.65	176.05	24.47	28.9	-4.59

error (RMSE), maximum absolute error, and maximum deformation are adopted to analyze the measurement error which are listed in Table I.

From Fig. 10 and Table I, strong agreement is demonstrated between the measured data and the observational data. In the four shape experiments, the maximum RMSE is 8.31 mm, and the maximum absolute error is 11.65 mm with the maximum deformation being 176.05 mm. The minimum RMSE is 2.35 mm, and the minimum absolute error is 1.59 mm with the maximum deformation being 61.99 mm. The tilt angle is in the range of $[-23^\circ, 29^\circ]$. There are two main reasons for error. First, the error of tilt angles which comes from the accelerometer. Second, the error corresponding to the front part of the curve could be additive, resulting in larger cumulative errors for the end of the curve, thus making it important to improve the accuracy at the front of the curve. In the test, with the increase in the deformation, the precision of structural shape reconstruction decreases. This is because the error almost increases with the tilt angles in the range of $[0^\circ, 30^\circ]$ and decreases in the range of $[-20^\circ, 0^\circ]$ after calibration.

VI. DISCUSSION

In the study, the sensor array is designed as a flat belt, and the x-axis of the array has the best deformation characteristics. The x-axis just coincides with the main subsidence direction, which is a two-dimensional displacement measurement. However, this is not to say that the flexible array is only suitable for measurements with a single direction. The displacement on y-axis can also be measured.²⁹ If the z-axis displacement and rotation around the z-axis is necessary, an additional instrument such as a magnetic sensor is required as a supplement. So, the MEMS sensor adopted in the study, MPU 9250, includes an accelerometer, gyro sensor, and magnetic sensor.

The IIC bus protocol is generally used for short distance communication. In order to extend the length of the array, one processor connects every eight segments, and the in-array microprocessors can collect and send signal data through a CAN bus protocol.

To improve the accuracy of the monitoring of subsidence, the accelerometer is calibrated by a least squares optimization model. The 9-parameter model (three for the offset \mathbf{o} and six elements in the sensitivity matrix \mathbf{S}) is adopted as it is based on the assumption that the sensitivity matrix is symmetric. Actually, a maximum of 12 parameters (three for the offset \mathbf{o} and nine elements in the sensitivity matrix \mathbf{S}) can be included in the model, when each element of \mathbf{S} is independent from the others. Using 12 parameters, the same accuracy of the

9-parameter model is achieved.¹¹ Therefore, the 9-parameter model is generally adopted.

Additionally, both the sensor array and the data processing method can be applied to seabed subsidence field monitoring. In shallow water, the array can be sealed by heat-shrinkable tube, while a high-pressure chamber for the sensor is required for waterproof and pressure resistance in deep sea. The monitoring system will be installed and tested in shallow water soon.

VII. CONCLUSIONS

The MEMS sensor array development is driven by the requirements of multi-point subsidence measurements. It has the advantages of anti-interference capability of noise, large deformation capacity, and automatic measurement. The key features are as follows.

- (1) The sensor array senses tilt information based on the gravity component and can accurately reflect the relationship between the measurement data and vertical displacement. The number and intervals of the measurement units can be flexibly customized to match the different operating conditions.
- (2) Design of the MEMS sensor array. The array is designed as a shape of a belt, which allows bends but resists twisting motions. It can have a large deformation capacity and help obtain deformation coupling between the array and the detected body.
- (3) Calibration and verification of the measurement result. To improve the accuracy of the displacement calculation, a calibration model of the tilt angle is presented. The model parameters are computed through nonlinear optimization, which is solved by the Levenberg-Marquardt algorithm. Experimental results show that the calibration model performs excellently with the maximum error of tilt angle being less than 1° in our applied measurement range ($-90^\circ, 90^\circ$). The accuracy of the displacement measurement was verified in laboratory tests, and the results indicate a strong agreement between the detected data and actual deformation with an accuracy of almost less than 1 cm (the array is 2.1 m in length).

ACKNOWLEDGMENTS

This study was supported by the National Key Research and Development Program of China (No. 2017YFC0307703) and the Natural Science Foundation of Zhejiang Province (No. Y17E090017).

- ¹Abdoun, T., Bennett, V., Danisch, L., and Barendse, M., “Real-time construction monitoring with a wireless shape-acceleration array system,” in *Proceedings of the GeoCongress Characterization, Monitoring, and Modeling of GeoSystems* (Geotechnical Special Publications, 2008), pp. 533–540.
- ²Arzu, A., Abdullah, K. M., Mert, E. A., Akgun, H., and Kockar, M. K., “Optical fiber technology to monitor slope movement,” in *Engineering Geology for Society and Territory*, edited by Lollino, G., Giordan, D., Crosta, G. B., Corominas, J., Azzam, R., Wasowski, J., and Sciarra, N. (Springer, Cham, Switzerland, 2015).
- ³Bennett, V., Abdoun, T., and Barendse, M., “Evaluation of soft clay field consolidation using mems-based in-place inclinometer–accelerometer array,” *Geotech. Test. J.* **38**(3), 20140048 (2015).
- ⁴Dasenbrock, D. D., Abdoun, T., and Bennett, V., “Real-time structural health monitoring of landslides and geotechnical assets with ShapeAccelArrays,” in *Geo-Frontiers Congress* (American Society of Civil Engineers, 2011), pp. 1585–1594.
- ⁵Frosio, I., Pedersini, F., and Borghese, N. A., “Autocalibration of MEMS accelerometers,” *IEEE Trans. Instrum. Meas.* **58**(6), 2034–2041 (2009).
- ⁶Frosio, I., Pedersini, F., and Borghese, N. A., “Autocalibration of triaxial MEMS accelerometers with automatic sensor model selection,” *IEEE Sens. J.* **12**(6), 2100–2108 (2012).
- ⁷Ha, D. W., Park, H. S., Choi, S. W., and Kim, Y., “A wireless MEMS-based inclinometer sensor node for structural health monitoring,” *Sensors* **13**(12), 16090–16104 (2013).
- ⁸Li, X. and He, S., “Progress in stability analysis of submarine slopes considering dissociation of gas hydrates,” *Environ. Earth Sci.* **66**(3), 741–747 (2012).
- ⁹Li, C., Fernandez-Steeger, T. M., Link, J. Á. B., May, M., and Azzam, R., “Use of MEMS accelerometers/inclinometers as a geotechnical monitoring method for ground subsidence,” *Acta Geodyn. Geomater.* **11**(4), 337–349 (2014).
- ¹⁰Lu, X. B., Chen, X. D., Lu, L., and Zhang, X. H., “Numerical simulation on the marine landslide due to gas hydrate dissociation,” *Environ. Earth Sci.* **76**(4), 172 (2017).
- ¹¹Madsen, K., Nielsen, H. B., and Tingleff, O., *Methods for Non-Linear Least Squares Problems* (IMM, Technical University of Denmark, Lyngby, Denmark, 2004).
- ¹²Miadro, R., Dacome, C., Mosconi, A., and Roncari, G., “Subsidence monitoring system for offshore applications: Technology scouting and feasibility studies,” *Proc. Int. Assoc. Hydrol. Sci.* **372**, 323–330 (2015).
- ¹³Miljkovic, A. V., “Worldwide distribution of submarine mud volcanoes and associated gas hydrates,” *Mar. Geol.* **167**(1–2), 29–42 (2000).
- ¹⁴Park, J. W., Sim, S. H., Jung, H. J., and Spencer, B. F., “Development of a wireless displacement measurement system using acceleration responses,” *Sensors* **13**(7), 8377–8392 (2013).
- ¹⁵Pei, H., Peng, C., Yin, J., Zhu, H., Chen, X., and Pei, L., “Monitoring and warning of landslides and debris flows using an optical fiber sensor technology,” *J. Mt. Sci.* **8**(5), 728–738 (2011).
- ¹⁶Pei, H. F., Yin, J. H., Zhu, H. H., Hong, C. Y., Jin, W., and Xu, D. S., “Monitoring of lateral displacements of a slope using a series of special fibre bragg grating-based in-place inclinometers,” *Meas. Sci. Technol.* **23**(2), 025007 (2012).
- ¹⁷Polster, A., Fabian, M., and Villinger, H., “Effective resolution and drift of paroscientific pressure sensors derived from long-term seafloor measurements,” *Geochem., Geophys., Geosyst.* **10**(8), 4918, <https://doi.org/10.1029/2009gc002532> (2009).
- ¹⁸Qian, J., Fang, B., Yang, W., Luan, X., and Nan, H., “Accurate tilt sensing with linear model,” *IEEE Sens. J.* **11**(10), 2301–2309 (2011).
- ¹⁹Saito, H. and Yokoyama, T., “Development of seafloor displacement monitoring system using a 3-component servo-accelerometer” in *OCEANS 2008-MTS/IEEE Kobe Techno-Ocean* (IEEE, 2008), pp. 1–4.
- ²⁰Segalini, A. and Carini, C., “Underground landslide displacement monitoring: A new mmes based device,” in *Landslide Science and Practice*, edited by Sassa, K. (Springer Berlin Heidelberg, 2013).
- ²¹Stenvold, T., Eiken, O., Zumberge, M., Sasagawa, G., and Nooner, S., “High-precision relative depth and subsidence mapping from seafloor water pressure measurements,” *Soc. Pet. Eng. J.* **11**(3), 380–389 (2006).
- ²²Uchimura, T., Towhata, I., Wang, L., Nishie, S., Yamaguchi, H., Seko, I., and Qiao, J. P., “Precaution and early warning of surface failure of slopes using tilt sensors,” *Soils Found.* **55**(5), 1086–1099 (2015).
- ²³Wang, Z., Jia, Y., Liu, X., Wang, D., Shan, H., Guo, L., and Wei, W., “*In situ* observation of storm-wave-induced seabed deformation with a submarine landslide monitoring system,” *Bull. Eng. Geol. Environ.* **7**, 1–12 (2017).
- ²⁴Xu, W. and Germanovich, L. N., “Excess pore pressure resulting from methane hydrate dissociation in marine sediments: A theoretical approach,” *J. Geophys. Res., B* **111**(B1), B01104, <https://doi.org/10.1029/2004jb003600> (2006).
- ²⁵Yang, W., Fang, B., Tang, Y. Y., Qian, J., Qin, X., and Yao, W., “A robust inclinometer system with accurate calibration of tilt and azimuth angles,” *IEEE Sens. J.* **13**(6), 2313–2321 (2013).
- ²⁶Yokoyama, T., Shimoyama, M., Matsuda, S., Tago, K., Takeshima, J., and Nakatsuka, Y., “Monitoring system of seafloor subsidence for methane hydrate production test,” in *18th Formation Evaluation Symposium of Japan* (SPWLA, 2012), pp. 1–6.
- ²⁷Yokoyama, T., Shimoyama, M., Matsuda, S., Tago, K., and Takeshima, J., “Monitoring system for seafloor deformation during methane hydrate production test,” in *Tenth ISOPE Ocean Mining and Gas Hydrates Symposium* (ISOPE, 2013), pp. 132–135.
- ²⁸Zhang, X. H., Lu, X. B., Li, Q. P., and Yao, H. Y., “Thermally induced evolution of phase transformations in gas hydrate sediment,” *Sci. China Phys., Mech. Astron.* **53**(8), 1530–1535 (2010).
- ²⁹Zhang, Y., Tang, H., Li, C., Lu, G., Cai, Y., Zhang, J., and Tan, F. L., “Design and testing of a flexible inclinometer probe for model tests of landslide deep displacement measurement,” *Sensors* **18**(1), 224 (2018).
- ³⁰Zhao, Z. and Shang, X., “Numeric simulation for the seabed deformation in the process of gas hydrate dissociated by depressurization,” in *International Conference on Information Computing and Applications* (Springer-Verlag Berlin, Berlin, Germany, 2010), pp. 296–303.